Vesicles and worm-like micelles: Structure, dynamics and transformations

P. A. Hassan*, Janaky Narayanan and C. Manohar[§,†]**

*Novel Materials and Structural Chemistry Division, Bhabha Atomic Research Centre, Mumbai 400 085, India
**Physics Department, R. J. College, Ghatkopar, Mumbai 400 086, India
[§]Chemical Engineering Department, Indian Institute of Technology, Powai, Mumbai 400 076, India

This paper reviews the concepts that have emerged in the area of spontaneously formed worm-like micelles and vesicles in cationic and anionic surfactant mixtures. The use of Rheology, Light scattering, Fluorescence Recovery After fringe Pattern Photobleaching (FRAPP) and Transient Electric Birefringence in characterizing worm-like micelles is described. Methods of interpreting the data and extracting relevant parameters like micellar breaking time and elastic moduli are illustrated by citing some examples.

CONVENTIONAL micelles are fluid aggregates of surfactants with shape and size decided by packing of individual surfactants. The main characteristics of such micelles are:

a) These micelles are stabilized by hydrophobic forces and head group repulsions (electrostatic and steric).
b) Each surfactant moves as in a fluid and the size, shape and aggregation numbers are decided by the packing parameter for the individual surfactant[1].
c) Length scales of these micelles are in 10–1000 Å.
d) The life times of these micelles are in milliseconds. On dilution below critical micelle concentration the aggregates disappear in milliseconds.

The realization that there could be micelles and aggregates of different type[2–4] is recent, though manifestations of unusual properties of such systems have been known for some time[5]. The classic example of such an 'abnormal' system is a solution containing cationic surfactant cetylpyridinium chloride (CPC) with sodium salicylate (SS) as the additive. These systems show strong viscoelastic effects even at extremely low volume fractions – a few millimolar concentrations[6]. Several representative and interesting features of these systems could be seen from Figure 1 which shows the 'zero-shear viscosity' of 100 mM CPC solution at 20°C as function of SS/surfactant ratio[7]. Notable features are observation of high viscosity even at extremely low concentrations and the existence of *two peaks* in the viscosity. The electron microscopic pictures of these highly viscoelastic solutions show the existence of entangled polymeric micelles of length of several microns! Two important developments, which gave clue to at least partial understanding of these features are:

a) SS is surface active and belongs to the class of anionic hydrotropes[8,9].
b) Observation of the formation of *two vesicle phases (low viscosity)* by Kaler *et al.*[10] in mixed cationic and anionic surfactant systems, one phase containing positively charged vesicles and the other one negatively charged.

Through this development it became clear that by mixing surfactants (hydrotropes) of opposite charges, cationic and anionic, but with varying chain lengths one can control the degree of precipitation of the surfactants to produce different supramolecular structures like vesicles and polymeric micelles[11–25]. One can also produce tubules, ribbons, etc. by controlling the solubility of surfactants[26,27]. This facilitates an easy control over the aggregate structure and hence it is possible to induce transformations from vesicles to micelles by a proper choice of additives which are cationic[28–30],

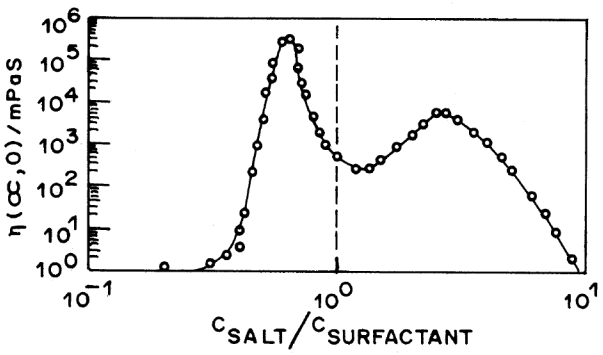

Figure 1. Zero shear viscosity of cationic surfactant CPC at 20°C as a function of sodium salicylate/surfactant ratio. These solutions show viscoelasticity. Note the existence of two peaks which is a common feature of cationic–anionic surfactant mixtures (adapted from ref. 7).

[†]For correspondence (e-mail: chittar@vsnl.com)

anionic[31–35] or neutral[36–38]. Although a number of early investigations were carried out on surfactant-mediated solubilization of vesicles due to its important implications in biochemistry, there are very few studies describing such vesicle–micelle transition induced by temperature[3,39,40].

A temperature-induced vesicle to micelle transition has been observed in the system of a new catanionic surfactant cetyltrimethylammonium 3-hydroxy naphthalene 2-carboxylate (CTAHNC)[3]. Horbaschek *et al.*[41] have shown, using calorimetry and conductivity measurements, that the vesicle-to-micelle transition occurs in this system at 45°C and is induced by melting of vesicle surfaces. At melting the ions are released from surfaces, giving a jump in conductivity at this point and if there are trapped ions in vesicles they are also released.

The vesicle to micelle transition in this system has been well characterized by several techniques like rheology, light scattering, NMR, fluorescence, small angle neutron scattering (SANS), etc. It has been shown that the vesicle to worm-like micelles transitions can be induced by temperature, additives and shear. Unlike polymers, these worm-like micelles break and reform and these characteristics show up in these experiments. Some of the methods that have emerged to characterize the networks formed by worm-like micelles are reviewed in the next few sections.

Theoretical models based on the concept of curvature elasticity of thin films or on molecular approaches have been proposed for micelle–vesicle transition in lipid–detergent mixtures[42–44]. These models can take into account the basic characteristics of these transitions, in particular the presence of a two-phase region consisting of coexisting vesicles and micelles. A similar model has also been proposed for vesicle to micelle transition[45] in cationic anionic mixtures and the key concept[46] is depicted in Figure 2. Cationic and anionic surfactants, in view of their strong interaction in polar region, form dimers and higher n-mers even at low concentrations. At any given temperature these are in thermal equilibrium. The relative concentrations of these species decide whether the system forms worms, vesicles or crystals. The relative concentrations can be estimated from extensions of the concepts of Bjerrum transitions in two dimensions[45]. Recent wide angle X-ray scattering studies have shown evidence to such melting of ion-pairs with temperature in catanionic surfactant solutions[26].

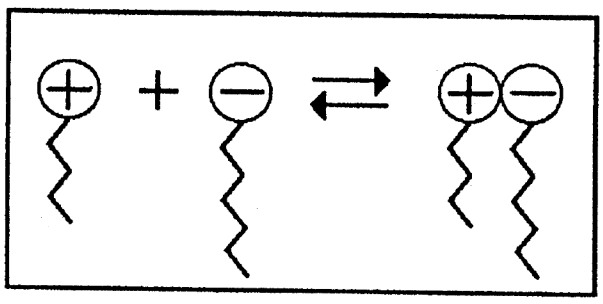

Figure 2. Strong coulomb interactions between the polar heads of cationic–anionic surfactants force them to form dimers, trimers, n-mers at interfaces of aggregates. Depending on the numbers, the bend elastic constant of the interface changes leading to formation of vesicles, worms, etc.[46].

Rheological studies

Rheological studies on worm-like micellar solutions provide useful information concerning phenomena such as micellar growth, entanglement, branching and shear-induced transitions. When a linear viscoelastic material is subjected to a sinusoidal deformation at an angular frequency, ω, the response of the material consists of a sinusoidal stress which is out of phase with the strain, the phase angle being δ. The sinusoidal deformation can be expressed as

$$\gamma(t) = \gamma_0 \exp(i\omega t), \tag{1}$$

where γ_0 is the strain amplitude.

Now the shear stress developed will also be sinusoidal with a phase angle δ, thus

$$\sigma(t) = \sigma_0 \exp(i[\omega t + \delta]), \tag{2}$$

For an oscillatory shear, we can define a complex shear modulus G^* as

$$G^* = \frac{\sigma(t)}{\gamma(t)} = \frac{\sigma_0}{\gamma_0}(\cos\delta + i\sin\delta) = G' + iG''. \tag{3}$$

G' and G'' are referred as the storage modulus and loss modulus respectively. Thus, from the phase angle δ and amplitudes of the shear stress and strain, one can calculate the storage modulus which represents the elastic response of the material and the loss modulus which represents the viscous response of the material. The response of the viscoelastic material under an applied shear may be characterized as linear or nonlinear depending on the amplitude of the shear.

Linear rheology

One of the prime quantities one infers from the linear rheological investigations is the stress relaxation time τ_R which is obtained by comparing the experimental data with a suitable model to describe the stress relaxation of polymeric micelles. Figure 3 *a* and *b* show the results of a typical linear rheological measurement for a semidilute solution of worm-like micelles and its Cole–Cole representation respectively (100 mM cetyltrimethyl ammonium tosylate (CTAT) at 30°C). At low

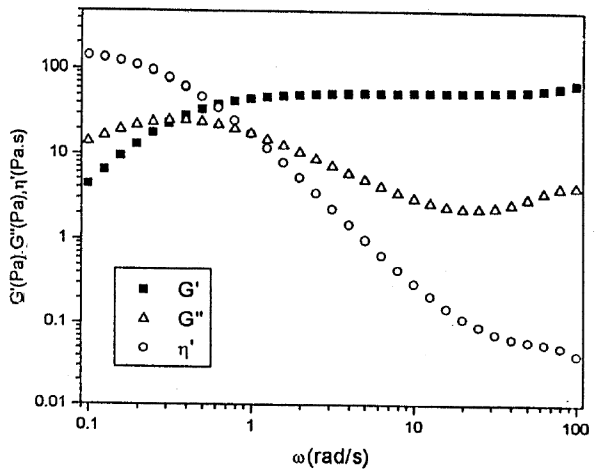

Figure 3 *a*. The storage modulus G', loss modulus G'' and viscosity η' as a function of frequency ω for a solution of 100 mM CTAT at 30°C.

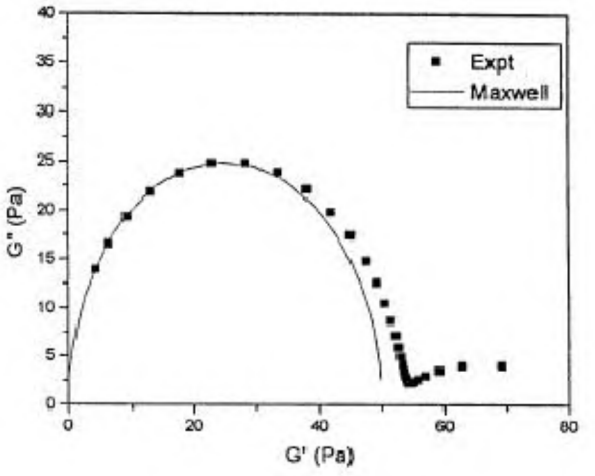

Figure 3 *b*. Cole–Cole plot for 100 mM CTAT at 30°C. The half circle (solid line) corresponds to an ideal Maxwell element with a unique relaxation time.

frequencies, the behaviour of the liquid is Maxwellian as observed by a semicircular shape of the Cole–Cole plot. For a Maxwell fluid, the variation of G' and G'' can be given as

$$G' = \frac{G(\omega\tau)^2}{1+(\omega\tau)^2} \quad \text{and} \quad G'' = \frac{G\omega\tau}{1+(\omega\tau)^2}, \tag{4}$$

where G is the shear modulus and τ is the characteristic relaxation time of the Maxwell element. This Maxwellian behaviour indicates a single exponential decay of the stress relaxation function. Now, we will see how a single exponential relaxation can be explained in the case of worm like micelles. Cates[47] proposed a simple model to explain the dynamics of stress relaxation in living polymer solutions. For living polymers, the possibility of breaking and recombination introduces new mechanism for stress relaxation, in addition to the reptation process. Within the framework of mean field model, the equilibrium length distributions $C(L)$ of a system of elongated micelles of length L is exponential with some mean length $\bar{L}$ and can be expressed as

$$C(L) \sim \frac{1}{\bar{L}^2}\exp(-L/\bar{L}). \tag{5}$$

Now it is helpful to introduce two characteristic times to describe the dynamics:

(a) τ_{rep}, the reptation time of an unbreakable chain of length $\bar{L}$; and (b) τ_b, the average time before such a chain breaks into two pieces as a result of the reversible scission process. Several regimes have been predicted depending on the relative ratio of the two time scales.

(i) When $\tau_b \gg \tau_{rep}$, the micelles behave like ordinary polydisperse unbreakable polymers with exponential polydispersity and the stress relaxation function, $\sigma(t)$ is very different from that of monodisperse polymers; one finds

$$\sigma(t) \sim \exp[-(t/\tau_{rep})^{1/4}] \tag{6}$$

as opposed to an almost pure exponential decay for monodisperse case.

(ii) When $\tau_b \ll \tau_{rep}$, chain breakage and recombination will both occur often for a typical chain, before it has disengaged from the tube by ordinary reptation. In this case, the reptation mechanism is short-circuited and the relaxation process will be monoexponential with a new time scale which is given as

$$\tau_R = (\tau_b\tau_{rep})^{1/2}. \tag{7}$$

This explains the observed single exponential behaviour of the system, because before a given tube segment relaxes, the chain occupying it typically undergoes many scission and recombination reactions, so that there is no memory of either the initial length of the chain or the position on the chain initially corresponding to the tube segment. Thus at low frequencies the behaviour of the liquid is Maxwellian and is ascertained by a semicircular shape of the Cole–Cole plot $G''(G')$. Such Maxwellian behaviour at low frequencies has been observed in many viscoelastic surfactant solutions[5,7]. But deviations from the half circle occur at a circular frequency ω of the order of the inverse of the breaking time of the micelles. Detailed results were obtained by Turner and Cates[48,49] from a computer simulation study of the coupled reaction/diffusion process for various values of the parameter $\zeta = \tau_b/\tau_{rep}$. The above results can be directly compared with the experimental curves, thus providing a direct estimate of the parameter ζ and hence τ_b.

The above studies do not take into account the dynamics at very high frequencies where one observes an apparent increase of the $G''(\omega)$. Later, the Poisson renewal model of Granek and Cates[50] has been applied to study the regimes involving small time scales where the dominant polymer motion is not reptation but either breathing (which arises from the tube length fluctuations) or the local Rouse like motion (arising from stretches of chain shorter than the entanglement length, l_e). This regime is characterized by an apparent turn up of both $G'(\omega)$ and $G''(\omega)$at high frequencies. This results in a minimum in the Cole–Cole representation of the dynamic modulus whose depth can be used to get an estimate of the average length $\bar{L}$. This picture applies when the entanglement length l_e is much larger than the persistence length l_p and the breaking time is much larger than the Rouse time τ_e. The frequency dependence of the complex shear modulus can thus be described with two parameters, namely the ratio $l_e/\bar{L}$ and ζ.

For flexible micelles the entanglement length l_e can be estimated from the relation[51,52]

$$G'_{\infty} = \frac{k_B T}{\xi^3} = \frac{k_B T}{l_e^{9/5} l_p^{6/5}}, \tag{8}$$

where $G'_{\infty} \approx G_0$ is the plateau modulus and ξ is the correlation length which gives the mesh size of the network. It was found that, provided $\tau_b \gg \tau_e$, the value of G'' at the dip obeys the relation

$$\frac{G''_{\min}}{G'_{\infty}} = \frac{l_e}{\bar{L}}. \tag{9}$$

From the values of $G''_{\min}$, G'_{∞} and l_e one can thus obtain an estimate of ξ as well as $\bar{L}$.

Further information regarding micellar branching and the effect of electrostatic interactions can be obtained from the scaling exponents of the various rheological parameters. The reptation theory of semidilute polymer solutions in good solvents predicts that[51]

$$G'_{\infty} \sim kT\phi^{2.3}, \tag{10}$$

where k is the Boltzmann constant, T is the absolute temperature and ϕ the volume fraction of the polymer. In the fast breaking limit, zero shear viscosity, η_0 scales as

$$\eta_0 \propto \phi^{3.5} \tag{11}$$

whereas in the slow breaking limit, η_0 scales as

$$\eta_0 \propto \phi^{5.3} \tag{12}$$

The scaling exponents are verified by Berret *et al.* on cetyl pyridinium chloride/sodium salicylate system[52]. The overall rheological data are found to scale with an exponent close to the predictions of the theory. The above scaling exponents were obtained assuming good solvent conditions and for fully screened electrostatic effects. But deviations from the above-mentioned scaling behaviour occurs due to the presence of electrostatic effects. It has been shown by Mackintosh *et al.*[53] that the growth behaviour of charged micelles differ from that of uncharged micelles and this in turn can reflect in the scaling exponents of the various rheological parameters. Thus, in the semidilute regime, the scaling of zero shear viscosity of charged micelles can be obtained as

$$\eta_0 \sim \phi^{7/2} \exp\left[\frac{E_C}{2kT}(1-(\phi^*/\phi)^{1/2})\right], \tag{13}$$

where E_C is the end cap energy and ϕ^* is the overlap concentration. The scaling exponents are also modified because of both the stiffness of the micelles and the formation of branches or connections in the network. The dynamics and the scaling behaviour of stiff rod-like micelles has also been studied by Cates *et al.*[54]. In some cases, the $\eta(\phi)$ increases sharply, then displays a maximum and decreases slowly thereafter[55,56]. Candau and co-workers[56] have explained these results based on the changes in end-cap energy with ϕ. The dynamics of linear flexible micelles has also been extended to the case of branched micelles by Lequeux[57]. It was shown that the general features of the stress relaxation function are maintained, except that for saturated networks the average lengths of the strand of the network varies as $\bar{L} \sim \phi^{-0.5}$. Thus the scaling behaviour of $G''_{\min}/G'_{\infty}$ with ϕ can be used to distinguish between linear micelles and branched micelles. In fact, there is direct evidence for the formation of micellar branches from cryo-transmission electron microscopic observations[58].

Nonlinear rheology

Nonlinear rheology describes the response of the material under large imposed shear. When the shear rate is very high, the stress induced in the sample varies nonlinearly. Worm-like micelles formed in certain surfactant solutions are known to show unusual nonlinear rheological behaviour. A nonlinear viscoelastic equation based on the reptation–reaction model has been derived by Spenley *et al.*[59]. It predicts a non-monotonic dependence of the stress on shear rate in simple steady flow. Shear banding is produced that may result in a plateau, σ_p of the shear stress in the experimentally measured flow curve under controlled mean strain rate. The limiting shear stress is predicted to be 0.67 G_0 and is in good agreement with the experimental results in

the semidilute regime[7]. The above behaviour contrasts with that obtained at higher concentrations and/or in presence of electrostatic interactions. It is observed that in the absence of salts, σ_p/G_0 is much less than the predicted value of 0.67 and it tends to a value close to 0.67 when electrostatic effects are screened out[60]. It appears that a very low value of σ_p/G_0, say less than 0.5, is obtained for systems with a surfactant concentration high enough to exhibit a local order.

Dynamic light scattering

In dynamic light scattering (DLS)[61], one measures the changes in the intensity of the scattered light $I_s(\tau)$ as a function of time and computes the second order correlation function which will be normalized with the long time correlation data $\langle I_s\rangle^2$. The normalized time correlation function of the scattered intensity, $g^{(2)}(\tau)$ can be written as

$$g^{(2)}(\tau) = \frac{\langle I_s(0) I_s(\tau)\rangle}{\langle I_s\rangle^2}. \tag{14}$$

For photo counts obeying Gaussian statistics, $g^{(2)}(\tau)$ is related to the first order correlation function of the electric field $g^{(1)}(\tau)$ by the Siegert relationship

$$g^{(2)}(\tau) = \beta + A\left|g^{(1)}(\tau)\right|^2, \tag{15}$$

where β is the baseline and A is an adjustable parameter dependent on the scattering geometry and independent of τ. For a suspension of monodisperse, rigid, spherical particles undergoing Brownian diffusion, the correlation function decays exponentially and is given as

$$g^{(1)}(\tau) = \exp(-Dq^2\tau), \tag{16}$$

where D is the translational diffusion coefficient and q the magnitude of the scattering wave vector.

In the dilute regime the measurement of the autocorrelation function of the scattered intensity allows one to estimate the translational diffusion coefficient of the micelles. In the semidilute regime, i.e. above the overlap concentration ϕ^*, the time correlation function of the scattered intensity is found to be bimodal in nature[62,63]. The fast and slowly decaying components are assigned as the diffusive gel mode and the relaxation mode respectively from their characteristic wave vector dependencies. It was shown[62] that the characteristic time of the fast gel mode is given by

$$\tau_f = \frac{K}{M_g + K}(D_c q^2)^{-1}, \tag{17}$$

where M_g and K are the gel modulus and osmotic modulus respectively and D_c is the cooperative diffusion coefficient. D_c is related to the hydrodynamic correlation length ξ_h

$$D_c = kT/(6\pi\eta\xi_h), \tag{18}$$

where η is the solvent viscosity. The scaling theory developed by de Gennes[64] for describing the static properties of flexible polymer chains can also be applied to dynamic scaling. In the semidilute regime, the corresponding collective diffusion constant D_c is independent of the length of the micelles, since the average length of the micelles is large compared to the mesh size ξ of the network. As ξ_h scales like ξ, D_c should increase with surfactant concentration in the semidilute regime. Thus DLS provides a convenient tool to probe the crossover between dilute and semidilute regimes. The applicability of the dynamic scaling laws is in semi-quantitative agreement with the experiment for cetyltrimethylammonium bromide/SS (CTAB/SS)[63] system for various ratios of CTAB/SS. At high q values of $q\xi_h \gg 1$, τ_f is predicted to be asymptotically proportional to q^{-3}, which reflects a single chain dynamics of a network strand. In order to check the applicability of the dynamic scaling law, a reduced plot of $\Gamma_f/D_c q^2$ is made against $q\xi_h$ for various ratios of CTAB/SS (where $\Gamma_f = 1/\tau_f$). All data are found to be superposed on one master curve and the curve was found to be in good agreement with the predictions.

The characteristic relaxation time for the slow mode arising from the coupling between stress and concentration fluctuation with time is given as

$$\tau_s = \tau_R \frac{M_g + K}{K}, \tag{19}$$

where τ_R is the terminal time of stress relaxation. The phenomenological theory developed by Doi and Onuki[65] explains the physics behind the dynamical coupling between concentration fluctuation and stress. It is argued that the mass flow or concentration fluctuation in the system creates deformation of the viscoelastic network, which produces gradient of the elastic stress. This gradient affects the diffusive motion of the polymer chains, resulting in slow decay of the concentration fluctuations as the stress relaxes. The above picture indicates that the fast mode is q^2 dependent whereas the slow mode is q independent. Experimental studies on cetylpyridinium chlorate ($CPClO_3$) in presence of sodium chlorate ($NaClO_3$)[62] and cetyltrimethylammonium bromide/SS (CTAB/SS)[63] system indicate good agreement with the above q dependencies. The concentration dependencies of ξ can be inferred from the measured D_c values which can also be obtained from the

measurements of shear modulus, G_0. Similarly the slow mode relaxation time provides an indirect estimate of the stress relaxation time which is usually obtained from dynamic rheological studies. Thus DLS can be used as a complementary technique to the measurement of some of the rheological parameters.

Transient electric birefringence

Under the effect of an applied electric field, anisometric micelles can be oriented if they have a permanent dipole moment and/or an anisotropy of electric polarizability. This alignment results in the micellar solution becoming optically anisotropic or birefringent, an effect known as Kerr effect or electric birefringence. In transient electric birefringence (TEB) experiments, a square electric pulse from a high voltage generator is applied to the solution. At the rising edge of the electric pulse, an electric birefringence $\Delta n = n_{\|}-n_{\perp}$ builds up in the solution and grows until a stationary value Δn_0 is reached. $n_{\|}$ and $n_{\perp}$ are respectively the refractive indices parallel and perpendicular to the direction of the applied field. On switching off the pulse, the birefringence decays with a characteristic time constant from which it is possible to extract information about the size and shape of the micelles. TEB is most sensitive to departure from spherical shape, as spherical particles show no birefringence unless distorted by the applied electric field. Hoffmann and co-workers[66,67] have used TEB studies to investigate the micellar growth in several surfactant solutions.

A typical set up used in the measurement of electric birefringence is shown in Figure 4. A beam of light from a 8 mw He–Ne laser (λ = 632.8 nm) is polarized at 45° with respect to the electric field applied across the Kerr cell. It passes through the solution in the Kerr cell, the path length (l) being 4 cm. High voltage electric pulses (up to 900 V) with duration ranging from 5 μs to 10 ms are applied across two polished steel electrodes separated by a distance of 2.2 mm. The rise and fall times of the pulses are typically < 0.2 μs. The light beam emerging parallel to the electrodes passes through a quarter wave plate whose slow axis is at $3\pi/4$ with respect to the electric field and then through the analyser before detection by a photodiode. The output of the optical detector is sampled with a transient recorder together with the high voltage electric pulse applied to the cell. The digital signals are processed by a computer.

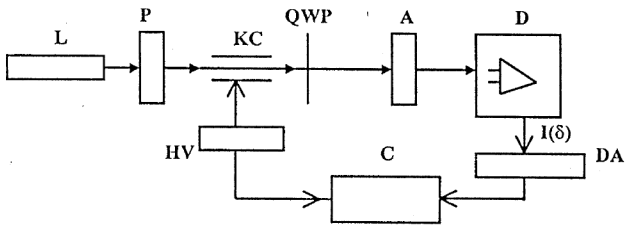

Figure 4. Schematic diagram of the experimental setup for Transient Electric Birefringence measurement. L: He–Ne laser, P: Polarizer, KC: Kerr cell, QWP: Quarter wave plate, A: Analyser D: Photodetector, DA: Differential Amplifier, HV: High voltage pulse generator, C: Computer.

If the analyser is rotated through an angle α from the crossed position towards the polarizer, the light intensity at the photodiode due to birefringence is given by[68]

$$I(\delta) = kI_0 \sin^2(\alpha + \delta/2). \tag{20}$$

I_0 is the incident intensity, k is a multiplication factor < 1 due to absorption and reflections in the optical parts and δ is the phase retardation in the components polarized parallel and perpendicular to the electric field.

$$\delta = \frac{2\pi}{\lambda} l\Delta n. \tag{21}$$

In the absence of the electric field, $\delta = 0$ and the intensity transmitted by the analyser is

$$I(0) = kI_0 \sin^2\alpha. \tag{22}$$

The change in light intensity at the photodiode due to birefringence = $\Delta I = I(\delta)-I(0)$ and the relative change in intensity is given by $\Delta I/I(0)$.

$$\text{If } \alpha = 45°, \frac{\Delta I}{I(0)} = \sin\delta. \tag{23}$$

A differential amplifier is used to measure ΔI. The electric pulse duration is kept long enough for the birefringence to reach a steady state value, Δn_0. The Kerr constant B is calculated from

$$B = \lim_{E\to 0}\left(\frac{\Delta n_0}{\lambda E^2}\right), \tag{24}$$

where E is the applied electric field. B can be positive, negative or zero depending on the chemical nature of the surfactant. Most of the dilute micellar systems show a negative birefringence, which is due to the intrinsic birefringence of the surfactant monomers. In surfactants like cetylpyridinium heptylsulfonate ($C_{16}PyC_7$), a positive birefringence is observed which arises from the difference of refractive index of the solvent and the rod-like micelles. Solutions of cetylpyridinium salicylate ($C_{16}PySal$) exhibit a negative birefringence, which shows that the sign of birefringence is strongly influenced by the optical anisotropy of the counterions. It is

possible by proper mixing of C_{16}PySal and $C_{16}PyC_7$ to change the sign of birefringence from positive to negative[66].

As the buildup of birefringence is a complicated function of field strength, usually the decay of the birefringence after the cessation of the electric pulse is analysed. For dilute surfactant solutions, the decay curve can be fitted to single exponential functions. The birefringence relaxation time τ is related to the rotational diffusion constant D_R of the particles though $\tau = (6D_R)^{-1}$. The expression of D_R for disks, rods and ellipsoids are known[69]. Deviations from single exponential decay of birefringence can be associated with polydispersity or intermicellar interactions.

In TEB experiments, anomalous relaxation is observed[70–72] in certain worm-like micellar solutions such as CTAT, near the overlap concentration, C^*. In dilute solutions ($C < C^*$), the birefringence reaches a single steady-state value when a square electric pulse of proper duration is applied. At the end of the pulse, the birefringence decays with a characteristic time constant (Figure 5 *a*). As the concentration is increased, one observes near C^*, a second component of the birefringence signal with opposite sign superimposed on the first one. This anomalous component exhibits a different magnitude and time constant with respect to the first one (Figure 5 *b*). With further increase in concentration, this second component becomes weaker and a third component appears with the same sign as the first one but with a much larger time constant (Figure 5 *c*). The sign of steady state birefringence reverts back to that found in dilute solutions. But now the solution is in a semidilute regime and it exhibits viscoelastic behaviour. By fitting the curves with

$$\Delta n(t) = \Delta n_1 \exp(-t/\tau_1) + \Delta n_2 \exp(-t/\tau_2) + \Delta n_3 \exp(-t/\tau_3), \quad (25)$$

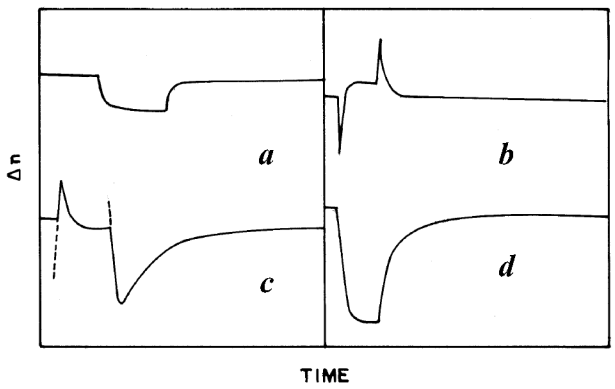

Figure 5. TEB signals for CTAT at 25°C. ***a***, C = 0.2%, E = 3×10^5 V/m; pulse duration = 25 μs; ***b***, C = 0.6%, E = 1.3×10^5 V/m; pulse duration = 1.5 ms; ***c***, C = 0.85%, E = 8.7×10^4 V/m; pulse duration = 4 ms; ***d***, C = 1.0%, E = 4.35×10^4 V/m; pulse duration = 15 ms.

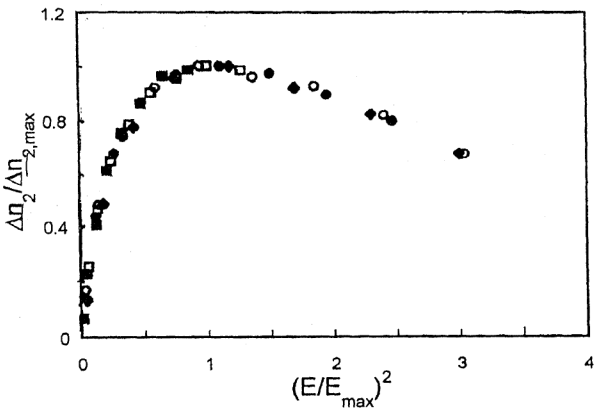

Figure 6. Master curve obtained by plotting $(\Delta n_2/\Delta n_{2,max})$ as a function of $(E/E_{max})^2$ for CTAT solution at 35°C for different concentrations; 0.7% (■); 0.8% (□); 0.9% (•);1.0% (O); 1.1% (◆).

the birefringence Δn's and the time constants τ's for each of the components can be evaluated.

From the first relaxation time τ_1 which dominates below C^*, the length of micelles L can be estimated. Δn_1 follows the Kerr law and the Kerr constant B_1 passes through a maximum near C^*. The anomalous birefringence Δn_2 appears for concentrations ranging from C_1 to C_2, with $C_1 < C^* < C_2$, and is nonlinear with E^2. It shows a maximum $\Delta n_{2,max}$ at E_{max} and decays to zero at higher fields. For a particular temperature, for all concentrations for which anomalous effect exists, Δn_2 values can be superposed on a master curve by plotting $(\Delta n_2/\Delta n_{2,max})$ vs $(E/E_{max})^2$ which suggests a universal behaviour of this effect (Figure 6). The third component appears above C^* and becomes more pronounced above C_2. For $C^* < C < C_2$, the variation of Δn_3 with E^2 is similar to that of Δn_1. But for $C > C_2$, Δn_3 assumes very large values and has a nonlinear behaviour with E^2. While the first time constant τ_1 is a few μs, τ_2 is few hundred μs and τ_3 is in ms.

According to Hoffmann *et al.*[70], the anomalous relaxation behaviour observed in long micelles is the result of overlapping of charged clouds of neighbouring micelles, which leads to the possibility of counterions diffusing from the double layer of one micelle to the other. This makes it difficult to electrically polarize the system along the axis of the rods in the direction of an applied field. However, it is possible to polarize the system perpendicular to the rod axis. This results in opposite birefringence. According to Cates[73], there exists a disk like local order in the system (pre-smectic ordering) due to steric hindrance between the particles near the overlap concentration. Since the disk-like clusters can only rotate as coherent units, under the influence of the field, the disks align parallel to the field while the particles forming the cluster are transversely oriented to it. This would lead to the anomaly in the birefringence signal. For CTAT micellar system[72] the

dimensions of these clusters are estimated in two different ways, using the rotational diffusion of disk-like clusters and considering the polarization of the charge cloud of the counterions. They are found to agree reasonably giving credence to both the models. At sufficiently strong fields, the local disk-like order would be destroyed. The disappearance of anomalous effect at high fields (Figure 6) is in accordance with this picture.

Fluorescence recovery after fringe pattern photobleaching

Self-diffusion of macromolecules is generally investigated with 'tracer' molecules, i.e. test molecules added in very small amounts to the medium. In fluorescence recovery after fringe pattern photobleaching (FRAPP) method, bleachable fluorescent molecules are used. The growth and entanglement of worm-like micelles and the crossover from dilute to semidilute regime can be investigated using FRAPP since the self-diffusion coefficient of the micelles is related to their size. Being a dynamic method, it can also throw light on the characteristic relaxation mechanisms involved in the viscoelastic behaviour of micellar systems.

The experimental setup for the FRAPP technique[74] is shown in Figure 7. In FRAPP, the self-diffusion coefficient of the fluorescent probes incorporated into the micelles is measured. These probes are also surfactant molecules with the polar head being a fluorescein

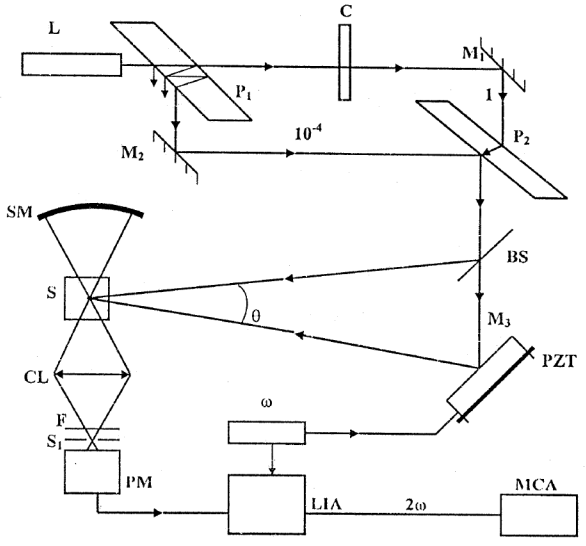

Figure 7. Schematic diagram of the experimental setup to study FRAPP (adapted from ref. 74). L: Laser, P_1, P_2: Glass plates producing two beams of unequal intensities, C: Chopper, M_1, M_2, M_3: Mirrors, BS: Beam splitter, PZT: Piezoelectric stack on which M_3 is mounted, SM: Spherical mirror, S: Sample, CL: High aperture collecting lens, F: Filter centered at the fluorescence wavelength, S_1: Shutter, PM: Photomultiplier, LIA: Lock-in-amplifier, MCA: Multichannel analyzer.

group. The mass ratio of the probe to surfactant is kept very low so that the probe molecules do not alter the micellar structure. In FRAPP experiment, a short pulse from a powerful laser beam (~ 400 mW), divided and superposed in a fringe geometry is used to bleach the fluorescence of the probes in the light regions. Subsequently, a less powerful laser beam (about 10^{-4} times less intense) forming the same fringe pattern is used to monitor the fluorescence signal. The diffusion of the probes from dark to light regions leads to the recovery of the fluorescence intensity. During the bleaching pulse duration (typically 50 ms) the shutter S_1 is closed and the piezoelectric device is not activated. During the observation period of the experiment, the chopper cuts the intense beam and the shutter S_1 is open. The piezoelectric device is activated to produce a phase modulated fluorescence signal, which is analysed with a lock-in amplifier. The diffusion coefficient is deduced by fitting the fluorescence recovery curve by an exponential function with a characteristic time constant, $\tau = i^2/4\pi^2 D$ where i is the fringe spacing (5–85 μm). The sample is kept in thermostated quartz cell of 1 mm path length. Details of the FRAPP technique and experimental set up have been published[74,75].

Figure 8 *a* (ref. 76) shows the variation of self-diffusion coefficient D of worm-like micelles formed from gemini surfactants 12-3-12, 12-2-12 and 16-4-16 with concentration, C. Gemini surfactants are dimeric cationic surfactants[77], alkanediyl-α-ω-*bis*(dimethylalkylammonium bromide) referred to as m-s-m surfactants (m and s being the carbon numbers of the side alkyl chains and of the alkanediyl spacer respectively). Three regimes can be distinctly seen:

(i) dilute regime ($C < C^*$), in which D remains more or less constant. A slight decrease in D can be related to the slow micellar growth. The hydrodynamic radius R_H in this range can be found using Stokes–Einstein equation, $D = kT/6\pi\eta R_H$, η being the solvent viscosity

(ii) semidilute regime ($C^* < C < C^{**}$), where D decreases drastically with C, which can be associated with entanglement of micelles

(iii) concentrated regime ($C > C^{**}$), in which D increases with C.

Similar behaviour is found in other micellar systems such as CTAT[78] and cetylpyridinium chlorate, $CPClO_3$[79]. It is interesting to find for all these systems, when the data D vs C are normalized in units of D_0 (the value of D for $C \to 0$) and C^* respectively, all curves collapse together showing a universal behaviour both in dilute and semidilute regimes (Figure 8 *b*). Combining Cates model[47] for polymer-like micelles and Mackintosh *et al.*[53] model for growth of charged micelles, the self-diffusion coefficient in the semidilute regime is shown to be[76],

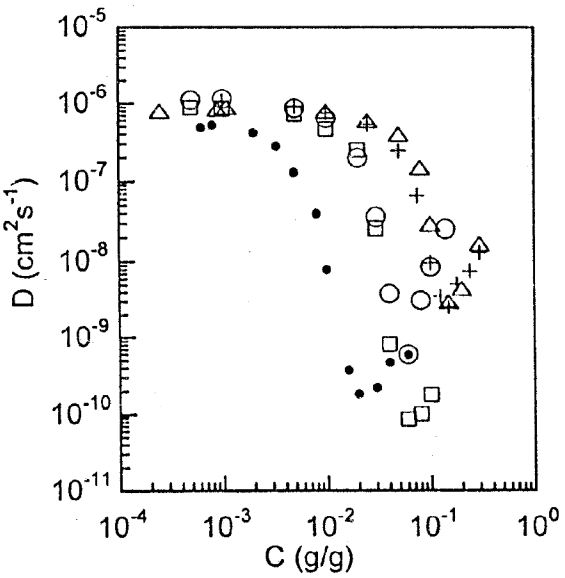

Figure 8 *a*. Variation of D with C for the salt-free surfactants 12-3-12 at 30°C (+), 12-2-12 at 35°C (O), 16-4-16 at 35°C (□), CTAT at 24.5°C (•) and $CPClO_3$ at 35°C(Δ).

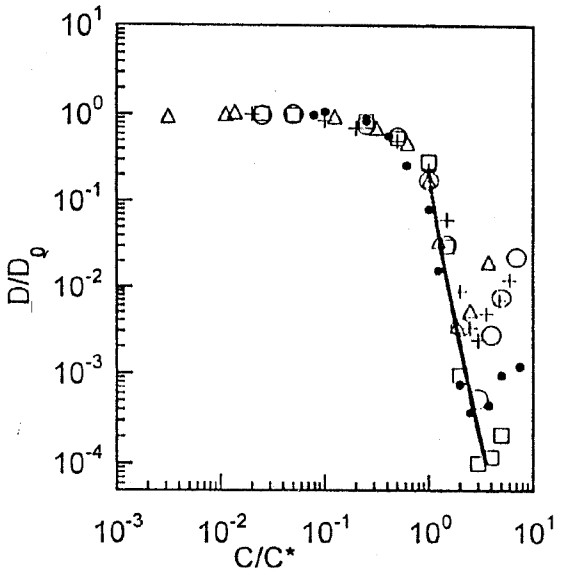

Figure 8 *b*. D/D_0 vs C/C^* for the surfactants represented by the same symbols as in Figure 8 *a*. The dotted line is the theoretical fit to the equation 28 with E_c = 33 kT.

$$D \sim D_0 C^{-5/3} \exp\left[\frac{-E_C}{3kT}(1-(C^*/C)^{1/2})\right], \qquad (26)$$

where E_C is the end-cap energy that favours the growth of the micelles. The universal behaviour of D is found to be due to the fact that the E_C values are remarkably similar in different systems (~ 30 kT). When excess salt is added, the electrostatic interactions are screened and C^* moves to very low values. In such cases one observes the power law behaviour, $D \sim C^{-\alpha}$, predicted by Turner *et al.*[80]. In the concentrated regime ($C>C^{**}$), D is found to increase with C as $D \sim C^{\beta}$. The possible role of progressive micellar branching above C^{**} is invoked to explain the increase of D with C[57,79].

Conclusions

In the last few years it has become clear that the vesicles and worm-like micelles in mixtures of cationic and anionic surfactants can be transformed into one another by controlling the relative ratios. This transformation from vesicle to worms appears to be decided by the surface rigidity. Worm-like micelles are quantitatively describable by living polymer models of Cates and others.

1. Israelachivili, J. N., Mitchell, D. J. and Ninham, B. W., *J. Chem. Soc., Faraday Trans. II*, 1976, **72**, 1526–1568.
2. Fuhrhop, J-H. and Helfrich.W., *Chem. Rev.*, 1993, **93**, 1565-1582.
3. Salkar, R. A., Hassan, P. A., Samant, S. D., Valaulikar, B. S., Kuma, R. V. V., Kern, F., Candau, S. J. and Manohar, C., *J. Chem. Soc., Chem. Comm.*, 1996, 1223–1224.
4. Manohar, C., in *Structure and Dynamics of Materials in Mesoscopic Domain* (eds Lal, M., Mashelkar, R. A., Kulkarni, B. D. and Naik, V. M.), Imperial College Press, London, 1999, pp. 252–258.
5. Cates, M. E. and Candau, S. J., *J. Phys. Condensed Matter*, 1990, **2**, 6869–6892.
6. Gravsholt, S., *J. Colloid Int. Sci.*, 1976, **57**, 575–577.
7. Rehage, H. and Hoffmann, H., *Mol. Phys.*, 1991, **74**, 933–973.
8. Manohar, C., Rao, U. R. K., Valaulikar, B. S. and Iyer, R. M., *J. Chem. Soc., Chem. Commun.*, 1986, 379–381.
9. Balasubramanian, D., Srinivas, V., Gaikar, V. G. and Sharma, M. M., *J. Phys. Chem.*, 1989, **93**, 3865–3870.
10. Kaler, E. W., Murthy, A. K., Rodriguez, S. Z. and Zasadzinski, J. A. N., *Science*, 1989, **145**, 1371–1374.
11. Bhattacharya, S. and De, S., *J. Chem. Soc., Chem. Comm.*, 1995, 651–652.
12. Bhattacharya, S. and De, S., *Langmuir*, 1999, **15**, 3400–3410
13. Bhattacharya, S., De, S. M. and Subramanian, M., *J. Org. Chem.*, 1998, **63**, 7640–7651.
14. Bhattacharya, S. and De, S., *J. Chem. Soc., Chem. Commun.*, 1996, 1283–1284.
15. Fukuda, H., Kawata, K., Okuda, H. and Regen, S. L., *J. Am. Chem. Soc.*, 1990, **112**, 1635–1637.
16. Kobuke, Y., Ueda, K. and Sokabe, M., *J. Am. Chem. Soc.*, 1992, **114**, 7618–7622.
17. Yatcilla, M. T., Herrington, K. L., Brasher, L. L., Kaler, E. W., Chiruvolu, S. and Zasadzinski, J. A., *J. Phys. Chem.*, 1996, **100**, 5874–5879.
18. Marques, E., Khan, A., de Graca Miguel, M. and Lindman, B., *J. Phys. Chem.*, 1993, **97**, 4729–4736.
19. Brasher, L. L., Herrington, K. L. and Kaler, E. W., *Langmuir*, 1995, **11**, 4267–4277.
20. Magid, L. J., Han, Z., Warr, G. G., Cassidy, M. A., Butler, P. D. and Hamilton, W. A., *J. Phys. Chem. B*, 1997, **101**, 7919–7927.
21. Mishra, B. K., Samant, S. D., Pradhan, P., Sushama, B., Mishra and Manohar, C., *Langmuir*, 1993, **9**, 894–898.
22. Carver, M., Smith, T. L., Gee, J. C., Delichere, A., Caponetti, E. and Magid, L. J., *Langmuir*, 1996, **12**, 691–698.
23. Kreke, P. J., Magid, L. J. and Gee, J. C., *Langmuir*, 1996, **12**, 699–705.

24. Bachofer, S. J. and Simonis, U., *Langmuir*, 1996, **12**, 1744–1754.
25. Long, M. A., Kaler, E. W. and Lee, S. P., *Biophys. J.*, 1994, **67**, 1733–1742.
26. Zemb, T., Dubois, M., Deme, B. and Gulikkrzywicki, T., *Science*, 1999, **283**, 816–819.
27. Oda, R., Huc, I., Schmutz, M., Candau, S. J. and Mackintosh, F. C., *Nature*, 1999, **399**, 566–569.
28. Edwards, K., Gustaffson, J., Almgren, M. and Karlsson, G., *J. Colloid. Int. Sci.*, 1993, **161**, 299–309.
29. Friberg, S. E., Campbell, S., Fei, L, Yang, H., Patel, R. and Aikens, P. A., *Coll. Surf. A*, 1997, **129–130**, 167–173.
30. Kaler, E. W., Herrigton, K. L., Murthy, A. K. and Zasadzinski, J. A. N., *J. Phys. Chem.*, 1992, **96**, 6698–6707.
31. Cohen, D. E., Thurston, G. M., Chamberlin, R. A., Benedek, G. B. and Carey, M. C., *Biochemistry*, 1998, **37**, 14798–14814.
32. Pedersen, J. S., Egelhaaf, S. U. and Schurtenberger, P., *J. Phys. Chem.*, 1995, **99**, 1299–1305.
33. de la Maza, A. and Parra, J. L., *Langmuir*, 1995, **11**, 2435–2441.
34. Egelhaaf, S. U. and Schurtenberger, P., *Phys. Rev. Lett.*, 1999, **82**, 2804–2807.
35. Egelhaaf, S. U. and, Schurtenberger, P., *Phys. B*, 1997, **234–236**, 276–278.
36. Oda, R., Bourdieu, L. and Schmutz, M., *J. Phys. Chem. B*, 1997, **101**, 5913–5916
37. Inoue, T., Motoyama, R., Miyakawa, K. and Shimozawa, R., *J. Colloid Interface Sci.*, 1993, **156**, 311–318.
38. Cariontaravella, B., Chopineau, J., Ollivon, M., Lesieur, S., *Langmuir*, 1998, **14**, 3767–3777.
39. Forte, L., Andrieux, K., Keller, G., Grabiellemadelmont, C., Lesieur, S., Paternostre, M., Ollivon, M., Bourgaux, C. and Lesieur, P., *J. Thermal Analysis Calorimetry*, 1998, **51**, 773–782.
40. Dubachev, G. E., Polozova, A. I., Simonova, T. N., Borovyagin, V. L., Demin, V. V. and Barsukov, L. I., *Biol. Membr.*, 1996, **13**, 100–109.
41. Horbaschek, K., Hoffmann, H. and Thunig, C., *J. Colloid. Int. Sci.*, 1998, **206**, 439– 456.
42. Andelman, D., Kozlov, M. M. and Helfriich, W. *Europhys. Lett.*, 1994, **25**, 231–236.
43. Fattal, D. R. , Andelman, D. and Ben-Shaul, A. *Langmuir*,1995, **11**, 1154–1161.
44. Kozlov, M. M., Lichtenberg, D. and Andelman, D. *J. Phys. Chem.*, 1997, **101**, 6600–6606.
45. Menon, S. V. G., Manohar, C. and Lequeux, F., *Chem. Phys. Lett.*, 1996, **263**, 727–732.
46. Salkar, R. A., Mukesh, D., Samant, S. D. and Manohar, C., *Langmuir*, 1998, **14**, 3778–3782.
47. Cates, M. E., *Macromolecules*, 1987, **20**, 2289–2296; *J. Phys. (Paris*), 1988, **49**, 1593–1600.
48. Turner, M. and Cates, M. E., *J. Phys. (Paris),* 1990, **51**, 307–316.
49. Cates, M. E. and Turner, M., *Europhys. Lett.,* 1990, **11**, 681–686.
50. Granek, R. and Cates, M. E., *J. Chem. Phys.*, 1992, **96**, 4758–4767.
51. Doi, M. and Edwards, S. F., *The Theory of Polymer Dynamics,* Clarendon Press, Oxford, 1986.
52. Berret J. F., Appell, J. and Porte, G., *Langmuir*, 1993, **9**, 2851–2854.
53. Mackintosh, F., Safran, S. and Pincus, P., *Euro. Phys. Lett.*, 1990, **12**, 697–702.
54. Cates, M. E., Marques, C. and Bouchaud, J. P., *J. Chem. Phys.,* 1991, **94**, 8529–8536.
55. Hassan, P. A., Valaulikar, B. S., Manohar, C., Kern, F., Bourdieu, L. and Candau, S. J., *Langmuir*, 1996, **12**, 4350–4357.
56. Kern, F., Lequeux, F., Zana, R. and Candau, S. J., *Langmuir*, 1994, **10**, 1714–1723.
57. Lequeux, F., *Europhys. Lett.*, 1992, **19**, 675–681.
58. Danino, D., Talmon, Y., Levy, H., Beinert, G. and Zana, R. *Science* 1995, **269**, 1420.
59. Spenley, N. A., Cates, M. E. and McLeish, T. C. B., *Phys. Rev. Lett.*, 1993, **71**, 939–942.
60. Oda, R., Narayanan, J., Hassan, P. A., Manohar, C., Salkar, R. A., Kern, F. and Candau, S. J., *Langmuir*, 1998, **14**, 4364–4372
61. Pecora, R., *Dynamic Light Scattering: Applications of Photon Correlation Spectroscopy*, Plenum Press, New York, 1985.
62. Buhler, E., Munch, J. P. and Candau, S. J., *Europhys. Lett.*, 1996, **34**, 251–255.
63. Nemoto, N., Kuwahara, M., Yao, M. and Osaki, K., *Langmuir*, 1995, **11**, 30–36.
64. de Gennes, P. G., *Scaling Concepts in Polymer Physics*, Cornel University Press, Ithaca, New York, 1979.
65. Doi, M. and Onuki, A., *J. Phys. II*, 1992, **2**, 1631–1656
66. Schorr, W. and Hoffmann, H., in *Physics of Amphiphiles: Micelles, Vesicles and Microemulsions* (eds Degiorgio, V. and Corti, M.), North Holland, Amsterdam, 1985, pp. 160–180 and references therein.
67. Zana, R., in *Surfactant Solutions: New Methods of Investigations* (ed. Zana, R.), Marcel Dekker, Inc., New York, 1987, pp. 453–458 and references therein.
68. Fredericq, E. and Houssier, C., *Electric Dichroism and Electric Birefrengence*, Clarendon Press, Oxford, UK, 1973.
69. Broersma, S., *J. Chem. Phys.*, 1960, **32**, 1626–1631.
70. Hoffmann, H., Kramer, U. and Thurn, H., *J. Phys. Chem.*, 1990, **94**, 2027–2033.
71. Oda, R., Lequeux, F. and Mendes, E., *J. Phys. II (France),* 1996, **6**, 1429–1439.
72. Narayanan, J., Mendes, E. and Manohar, C., *J. Phys. Chem.*, 1996, **100**, 18524–18529.
73. Cates, M. E., *J. Phys. II*, 1992, **2**, 1109–1119.
74. Ott, A., Morie, N., Urbach, W., Bouchaud, J. P. and Langevin, D., *J. Phys. IV*, 1993, **3**, 91–103.
75. Davoust, J., Devaux, P. and Leger, L., *EMBO J.*, 1982, **1**, 1233–1238.
76. Narayanan, J., Urbach, W., Langevin, D., Manohar, C. and Zana, R., *Phys. Rev. Lett.,* 1998, **81**, 228–231.
77. Zana, R., *Curr. Opin. Colloid Interface Sci.*, 1996, **1**, 566–571 and references therein.
78. Narayanan, J., Manohar, C., Langevin, D. and Urbach, W., *Langmuir,* 1997, **13**, 398–401.
79. Morie, N., Urbach, W. and Langevin, D., *Phys. Rev. E*, 1995, **51**, 2150–2156.
80. Turner, M. S., Marques, C. and Cates, M. E., *Langmuir*, 1993, **9**, 695–701.

ACKNOWLEDGEMENTS. We are grateful to Drs S. J. Candau, D. Langevin, W. Urbach, E. Mendes, F. Kern, F. Lequeux, R. Oda, R. Zana, S. V. G. Menon, S. D. Samant and R. A. Salkar for collaboration in the project sponsored by Indo-French Centre for Promotion of Advanced Research.